Advances in Complex Systems, Vol. 4, No. 4 (2001) 509–522

THE FOUR AVALANCHE FRONTS: A TEST CASE FOR GRANULAR SURFACE FLOW MODELING

STÉPHANE DOUADY, BRUNO ANDREOTTI, PIERRE CLADÉ and ADRIAN DAERR
Laboratoire de Physique Statistique de l'E.N.S.,
24 rue Lhomond, F-75005 Paris, France

Received 11 September 2001
Accepted 30 November 2001

Granular surface flows have still to be fully modelled. Here, we present the four types of front that can be observed in avalanches. These strongly inhomogeneous and unsteady flows are very sensitive test cases for the different types of model. We show that, at least qualitatively for the moment, the model we propose, based on the analysis of the motion of a single grain and layers of grains, can reproduce the different characteristics of these four fronts.

Keywords: Avalanche fronts; St Venant equations; granular surface flow; velocity profile; sub-critical bifurcation; inelasticity; non-local shocks; trapping.

1. Introduction

With its ubiquity and practical importance, it is surprising that granular surface flows have not yet been described as clearly and completely as has been done long ago for liquid flows. One reason may be that the physical mechanisms at work in the flowing granular layer are different enough from the liquid case, and yet hardly described. To investigate these mechanisms a first step is to look at the motion of a single grain (Sec. 2). This already provides many clues of the essential physical mechanisms, namely inelastic collisions and trapping, leading to a strong sub-critical bifurcation between motion and rest [22].

A second step can then be to look at layers of grains flowing one above the other (Sec. 3). In this case we have the same effects as for a single grain (inelastic collisions and trapping), but we also find an essential effect: the non-locality of the collisions. This non-locality of the shocks explains the otherwise surprising linear velocity profile, and its combination with the trapping gives the depth selection of the surface flow [2].

From these observations, and other experimental ones, we propose a model [12]. In Sec. 4 we compare it with other propositions and possibilities. Then, we present the different types of fronts that can be observed in avalanches, and show how their different characteristics point to particular aspects that have to be present in a model trying to describe them (Sec. 5). Finally, we conclude with future work.

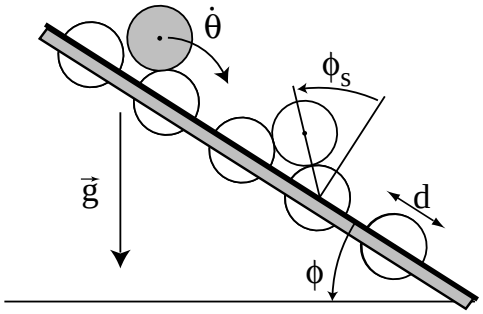

Fig. 1. Schematic set-up of the single bead experiment with notations.

2. The Motion of a Single Grain

A bead (in practice, a cylinder) placed on a row of identical beads presents several states (Fig. 1). The first is static equilibrium, when the bead is trapped in the hole in-between the beads underneath. If the row of beads is tilted by an angle ϕ, this bead remains static up to the angle at which the trap disappears. The bead will then spontaneously start to roll down. This defines the starting angle ϕ_{s} (usually referred as the static angle).

Another possible state is to have the bead rolling down indefinitely. Experimentally, it quickly reaches a constant mean velocity [14, 24]. If the angle of the row is decreased, this periodic motion abruptly becomes impossible below a second lower angle, the stopping angle ϕ_{d} (usually referred as the dynamical angle).

Analysis of the motion [22] shows that the bead rolls on those underneath, without sliding or jumping (for not too large an angle). During rolling it gains kinetic energy $\dot{\theta}^2_{\mathrm{down}} = \dot{\theta}^2_{\mathrm{up}} + 2\alpha^2 \frac{g}{d} \sin\phi_{\mathrm{s}} \sin\phi$, where α is related to the ratio of potential energy transferred into translation kinetic energy and the angular momentum. Then, it collides with the next bead. Even though the materials used are not completely inelastic (for instance, steel), we do not observe any rebound, but rather a perfectly inelastic normal collision. There remains some tangential velocity, and also part of the angular momentum is transformed into tangential kinetic energy. The bead thus starts rolling on the next bead, with a new angular velocity given by $\dot{\theta}_{\mathrm{after}} = \rho\dot{\theta}_{\mathrm{before}}$ where ρ (of the order of $1/2$) is the coefficient describing the loss of kinetic energy in the shock.[a]

This motion quickly leads to a constant angular velocity:

$$\dot{\theta}_l = \beta\sqrt{\frac{g\sin\phi}{d}}\,, \tag{2.1}$$

[a]This perfectly inelastic normal shock can be interpreted as the signature of an inelastic collapse; it makes a small rebound, but then an infinite number of small rebounds in a small finite time. It would be interesting to look precisely at the real shocks as carefully done by Zippelius *et al.* (this volume).

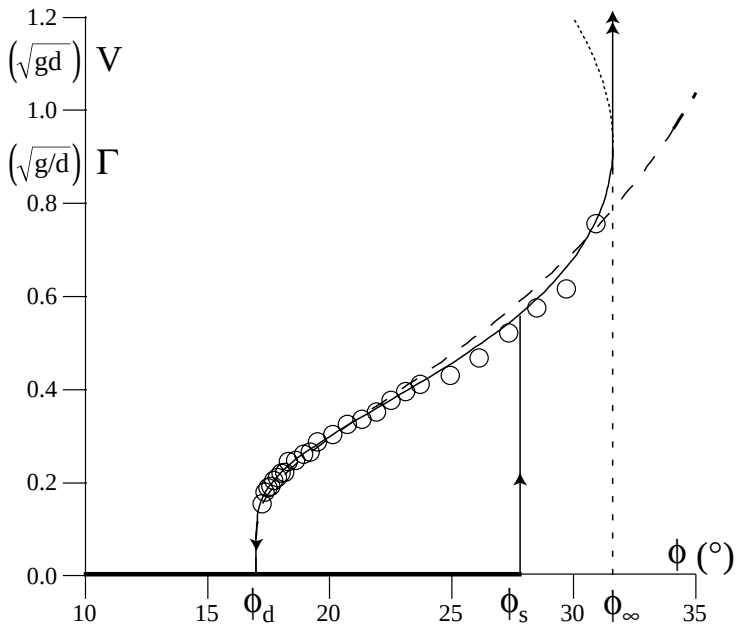

Fig. 2. Mean velocity for a single bead V. Assuming this is the relative layer velocity, it also corresponds to the velocity gradient $\Gamma = V/d$, where d is the bead diameter.

with $\beta = \alpha\rho\sqrt{2\sin\phi_s/(1-\rho^2)}$. We can see that this limit angular velocity is far from the mean velocity experimentally observed (cf. Fig. 2). The main difference is that no bead motion is observed below ϕ_d, and clearly not down to a horizontal row ($\Phi = 0$). This comes simply from the fact that even if the beads have a non-zero angular velocity after one shock, it will not necessarily go down to the next dip; in-between the two dips it has to pass above the bead. When the bumpy line angle is decreased, the limit angular velocity decreases. At the same time, the height above which it has to pass (the trapping height) increases; then comes an angle for which this limit angular velocity is not enough to escape from the trap, and this explains the origin of ϕ_d. Just above this angle, the bead slows down infinitely when passing above the one underneath, so the mean bead velocity goes abruptly to zero.

If the bead motion above the trap is numerically integrated, the experimental velocity is well reproduced (Fig. 2). This constant velocity regime ends at an upper angle ϕ_∞. Slightly below this value, the bead has too large an angular velocity so that just before a collision it stops rolling, takes off and simply jumps straight forward. The next collision occurs more tangentially, the loss of normal velocity is reduced, hence a larger mean velocity. At ϕ_∞, the bead even starts to jump above the following bead. It then makes a longer way down before the next collision, transferring more potential energy into kinetic energy, and thus making the next jump longer, and so on. As a result, the bead accelerates indefinitely.

In contrast to the previous formula (Eq. (2.1)), a good fit of the mean (macroscopic) velocity is given by

$$V = \gamma\sqrt{gd}\Big/ \ln\left(\frac{\tan\phi_\infty - \tan\phi_\mathrm{d}}{\tan\phi - \tan\phi_\mathrm{d}}\right), \tag{2.2}$$

with γ of the order of 0.4. However, with this formula, the fitted value for ϕ_∞ is too large and the divergence too slow (long dashed line) compared to experiment (see Fig. 2). To be closer to measurements, we add an upper unstable branch (dotted curve).

We can also look at the transients leading to this mean velocity, i.e. to the apparent forces acting on the bead. The measurements [22] give a force of the form:

$$F = \sigma g(\sin\phi - \mu\cos\phi) - \kappa\frac{V^2}{d}\,. \tag{2.3}$$

The effect of the collisions thus corresponds to a Bagnold type of term, as it should be, the shocks dissipating a part of V with a frequency V/d [5]. The driving force is to a first approximation a force proportional to the gravity (but smaller than its projection along the beads row). It is striking to see that a friction force also spontaneously appears with a friction coefficient μ.[b]

3. The Motion of Layers of Grains

How can we go from the motion of one bead to the propagation of an avalanche? The next step can be to look at the motion of superposed layers of beads. Even if it is difficult to do it experimentally with rigid layers, we can still turn to numerical simulations. We thus consider layers of periodic beads as sketched in Fig. 3. We assume the same motion as previously: each bead rolls without sliding on the ones underneath.

The crucial assumption concerns the shocks, when a bead in one layer collides with the one underneath. The assumption used for liquids, by Bagnold as well, is that the exchange of momentum is local, affecting only the two layers involved in the collision. In the case of liquids, the frequency of shocks is related to thermal agitation, while with grains, the frequency of shocks comes from the motion of the grains themselves. This gives the viscous or Bagnold stress, respectively. In both cases, the characteristics are the positive curvature of the velocity profile, the fact that the velocity derivative is null at the free surface (where no stress is exerted), and to flow down to the bottom, as sketched in Figs. 4(b) and (c).

Here, the main problem is precisely to model a surface flow, i.e. only a thin flow of grains on a remaining static layer (Fig. 4(a)). In our model, the beads are always rolling above one another, so they are always in contact (cf. Fig. 3). So when there is a shock, it is not just one bead colliding with another bead, but a small

[b]By setting this force to zero, we should recover the mean velocity. This is correct for the central range; this fit does not extend close to ϕ_∞, and the observed cut-off is sharper ($\mu < \tan\phi_\mathrm{d}$).

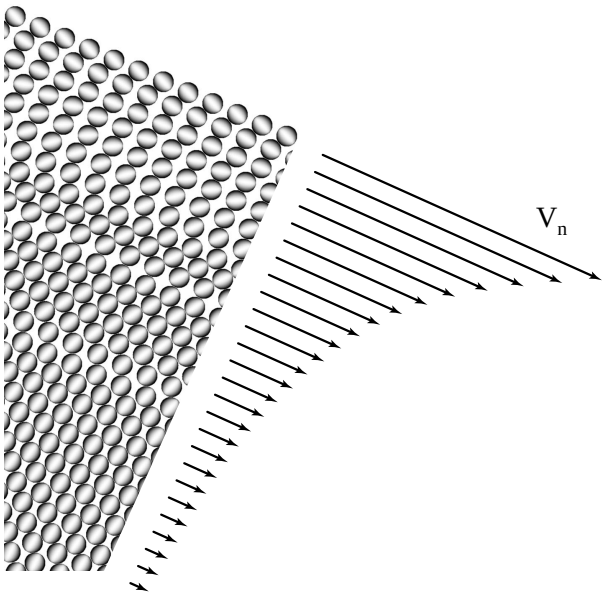

Fig. 3. A sketch of the flowing layers at one moment of their motion, with the resulting mean velocity profile.

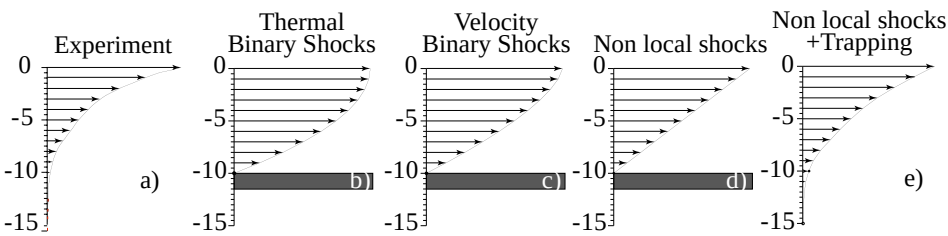

Fig. 4. Types of velocity profiles: (a) as experimentally observed using PIV, (b) with thermally induced binary shocks (viscous fluid), (c) with binary shocks induced by the motion itself (Bagnold's profile), (d) with non-local shocks in connected grains (this layer model), and (e) as obtained with this layer model.

column of beads colliding with another column of beads, the latter going down to the bottom. In this case the transfer of momentum is complex and depends on the angular position of the beads along these columns.

Simulating this model numerically gives the velocity profiles of Fig. 3 [2]. What we observe is precisely a flow only on the upper part for a small tilt angle. The flow depth increases with the inclination angle, eventually reaching the bottom above a given one. The velocity profile looks very close to those observed experimentally (Figs. 4(a) and (e) [6, 23]): roughly a linear velocity profile, followed by a slow creeping tail. This slow deformation tail has been carefully studied in Ref. 16. Komatsu *et al.* have shown that it is an exponential with a characteristic length of

five beads, independent of what is flowing above. This is very reminiscent of the exponential deformation observed in shear experiments (see Losert or Nagel, this volume). In other words, it seems that we just observe a flowing layer with a linear velocity profile which shears a static pile underneath.

If we look at the velocity gradient of this linear velocity profile, we find that it simply corresponds to the velocity of a single bead above a static layer [2] — roughly as if each layer of grain were rolling on a static underneath layer, with purely normal inelastic collisions [23]. This apparent inelasticity comes from the non-locality of the shocks: the momentum is transmitted down through the column underneath, so it looks as if it was dissipated, exactly as the momentum of a single bead is transmitted through the static bead, the plane, the table and the lab, down to the earth.

To further understand the selection of flow depth, we have to take into account the fact that one layer, to go above the layer underneath and fall into the next dip, has to lift up all the layers lying on it. In other words, the amplitude of the potential trapping increases linearly with depth. Now the shocks occurring above give only part of their momentum to this layer as some is still transmitted further down. The momentum transmitted thus increases with depth, but not as quickly as the trapping. So for a given angle, the condition that the shocks give enough momentum to pass the trapping selects a particular flowing depth.[c]

This roughly linear velocity profile observed in surface flows seems to be in contradiction with experiments and numerical simulations of granular flows on rough planes, showing rather a Bagnold type of velocity profile [1, 4, 21]. A possible reduction of this discrepancy is to point out two differences: the chute experiments are done for angles largely above the ones at which surface flows are considered; the boundary condition (hard rough bottom) is very different from the soft plastically deforming pile. From both these differences an interpretation is then that chute flows are slightly more diluted than surface flows, so that the contact chains could then be finite in length, and we may recover a Bagnold type of velocity profile. A way to check this interpretation would be to look at the characteristic length in the stress that can be derived from the velocity profile. This length should not be the grain diameter as in the Bagnold expression (see Hasley, this volume), but rather the typical chain length.

The presence of these contact chains giving rise to non-local shocks is precisely the idea underlying present models built to recover the characteristics of the chute velocity profiles [15, 18]. This is also the introduction of a non-local length scale (simply the depth of the flow) in front of the Bagnold shear stress that allows Khakhar (this volume) to recover not only the linear velocity profile but also the good scaling.

[c]The fact that the transferred momentum is constantly fluctuating, and that the beads in the sheared exponential tail wriggles before suddenly jumping over from time to time is very reminiscent of the model of thermal activation proposed by Pouliquen (this volume).

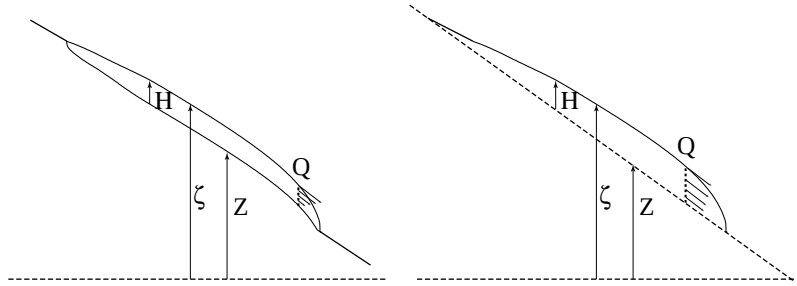

Fig. 5. Sketch and notations for a surface flow over a thick static pile (left) and a flow down to a fixed bottom (right).

4. Modeling

Looking at a single bead and layers of beads helps to understand the hysteresis, the apparent forces, and the particular velocity profile. Now a macroscopic modeling of the whole surface flow can be done using the formalism first introduced by St-Venant [11], integrating the equations of motion vertically. In the case of a flowing layer, as shown in Fig. 5, we obtain the general equations from mass and momentum conservation:

$$\partial_t \zeta + \partial_x Q = 0\,, \tag{4.1}$$

$$\partial_t Q + \partial_x E = \frac{1}{\rho} F\,. \tag{4.2}$$

All the terms are vertical integrals; the free surface elevation ζ is the integral of 1, the flux Q of the velocity, the overall energy E of the velocity square and F of the resulting forces. These two equations are exact and quite general. All the particularities and approximations come from the various possible expressions of the different terms. In the case of a surface flow as in Fig. 5 (left), the unknowns are: the free surface ζ, the flowing depth H and the mean velocity of the flowing layer U (simply related to the flux by $Q = UH$). We see that we have only two equations for three unknowns, so that at least one relation is missing.

4.1. *Fixed bottom*

A first solution is to consider flows down to a fixed bottom Z (Fig. 5, right). Then, the free surface is directly linked to the flowing height, $\zeta = Z + H$, and the two previous equations are enough to find the two remaining unknowns H and U. The first equation (4.1) gives the flowing depth H. The second (4.2) gives the mean velocity U, using $\partial_t Q = H\partial_t U + U\partial_t H$ and that $\partial_t H$ is given by the first equation.

Historically, this modeling was first used to study *flood waves* in rivers. In this case the flux Q is assumed to be known as a function of the local flowing height (derived from the local cross-sections of the river and/or flow calibrations). Then, only the first mass conservation equation (4.1) is enough to solve the problem, with the characteristics method, for instance [26].

Another classical use of these equations is for thin fluid layers. A first case is to assume a purely inviscid fluid (the shallow water approximation). Then, the velocity profile is a constant one (plug flow), the fluid layer just sliding as a whole on the bottom (so that $E = U^2 H$). The force is just derived from gravity and pressure (with at this place approximations of a thin, slowly varying layer). A second case is on the contrary to assume a very viscous fluid (the lubrification theory). The velocity profile is then half of a parabola (with curvature given by viscosity), as shown in Fig. 4, and there is a viscous force.

This fixed bottom approximation was also used in the case of granular flows. A first model by Savage and Hutter [25] is similar to the thin fluid film approximation, except that a friction force between the flowing layer and the bottom is added. Pouliquen [19, 20] has further refined this model by putting an effective force derived from his measurements of granular flows on a rough plane. This is very similar to the flood wave studies, using measurements in constant stable flows to predict non-uniform ones.

4.2. *Free bottom* (*thick pile*)

Few models have been written for the case of flow on an otherwise static pile. The first was proposed by BCRE [7], and later modified by BRdG [8]. As in the previous models, it assumes a plug flow (constant velocity profile), but there still remains three unknowns. So the velocity itself is assumed to be constant. The first equation (4.1) then gives an equation for the free surface ζ and the second (4.2) for the flow depth H, as now $\partial_t Q = U \partial_t H$. In other words, if the flowing layer wants to gain (lose) momentum, it simply increases (decreases) its thickness. The model was not presented in this way, so that the left part of the second equation was not recognized as deriving from a physical force. However, it corresponds roughly to a constant friction force. A model with two equations was also proposed by Mehta *et al.* [17], but it seems to be more difficult to translate into this St-Venant framework.

For our part we proposed, as well as Khakhar (this volume), a model using experimental results as those described above. So we rather assume a linear velocity profile [3]. Then, as above, we need another relation, to fix one unknown. So we assume that the velocity gradient Γ is locally constant and equal to that of a single bead in the same local conditions. We thus relate the mean velocity to the flowing depth, $U = \frac{1}{2}\Gamma H$, and $E = \frac{1}{3}\Gamma^2 H^3$. If the flowing layer wants to gain (lose) momentum, it now increases (decreases) both its mean velocity and depth, keeping its local velocity gradient unchanged. We also assume directly an hysteresis between static and dynamical friction forces with a typical transition depth (Fig. 6).

With these assumptions, the model summarizes as

$$\partial_t \zeta + 2U \partial_x H = 0\,, \tag{4.3}$$

$$\partial_t H + 2U \partial_x H = \frac{g}{\Gamma}(\tan\phi - \mu(H))\,, \tag{4.4}$$

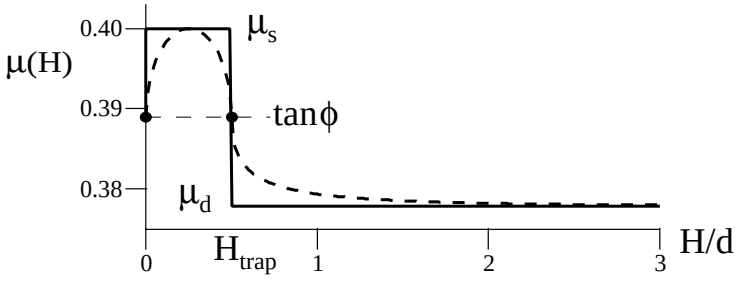

Fig. 6. Variation of the friction coefficient with flowing depth. Below a trapping height H_{trap}, of the order of one grain diameter, the friction coefficient exchanges from dynamical to static.

with $U = 1/2\Gamma H$, Γ as shown in Fig. 2, and $\mu(H)$ as in Fig. 6, and ϕ the local surface slope. The factor two in the advective terms comes from the linear velocity profile. This model can be checked in the case of stationary flows. This is what is done by Khakhar (this volume), but also Bonamy [6] for instance, with encouraging results. But we also want to check it for more demanding cases, namely transients and unstable situations. Apart from our work on the avalanches on a rough plane ([9, 10]), we will discuss here another type of strongly inhomogeneous and unsteady flows.

5. The Four Fronts of Avalanches

When sand is poured at the top of a pile with a small enough flux, it accumulates and eventually an avalanche starts. This avalanche front is the intuitive one. At a certain place, we observe the transition from a static surface to a flowing one, and the front goes down so we call this front the "start-down" front (Fig. 7(a)). When this front reaches the end of the pile, it spreads and stops. There is then a stopping front moving upward (Fig. 7(b)). When this "stop-up" front reaches the top of the pile, the sand accumulates again and so we have successive avalanches starting down and stopping up.

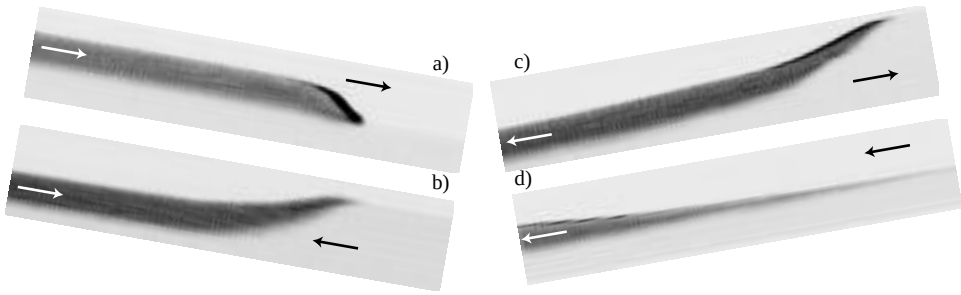

Fig. 7. The four types of fronts as observed with image differences.

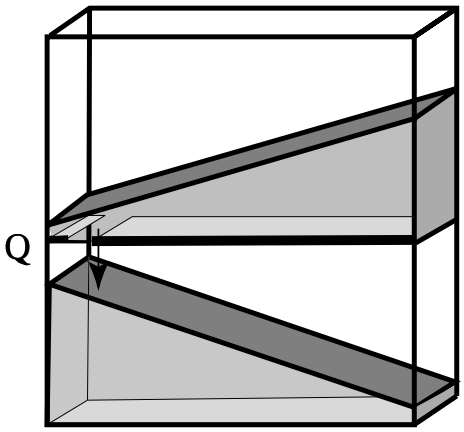

Fig. 8. Schema of the half flat hourglass experiment: the upper part is emptying into the lower part, with a fixed flux Q.

If we make the symmetric of this classical experiment, i.e. a sand pile emptying at its lower end, we also observe two other fronts. The complete experiment, with an upper flat silo emptying and a lower one filling up, could be described as a "half flat hourglass" (Fig. 8). In the upper part, the sand goes out at the foot of the sand pile, and it creates an increasing step. When this step is steep enough, the upper static grains start to roll down, and we observe a "start-up" front (Fig. 7(c)). When it has reached the top end of the pile, it also flattens and stops. We then observe a "stop-down" front (Fig. 7(d)). These four fronts are the four possible fronts either starting or stopping, either moving up or down.

These four fronts have different characteristics. The "start-down" and "start-up" fronts are sharp. We can also see that the "start-down" front sharpens with time, but tends towards a fixed shape. On the other hand, the "stop-down" and "stop-up" fronts are flat, and we can see them flattening with time. These observations are already very restrictive for possible models.

5.1. *Velocity profile*

The evolution of the front shapes depends first on the velocity profile inside the flowing layers. For a plug flow, the shapes are translated without any change at first order in time. The possible shape evolution is only second order in time, due to the effects of a force depending on the flowing height (pressure, for instance). This results in an effective diffusion of the flowing height. So it would flatten the "start-down" front, for instance.

In contrast, the effect of a non-constant velocity profile is first order in time, due to the advective term of the mass conservation equation (Eq. (4.3)). If the mean velocity U increases with flow depth H, then the "start-down" front precisely sharpens with time, and evolves toward breakdown and shock formation. The

"stop-down" front will also flatten continuously with time. Thus, the observations point toward a mean velocity increasing with flow depth.[d]

5.2. *Starting fronts shapes*

If an increasing velocity profile is assumed, the mean velocity usually goes to zero for a null flowing height. Then, a simple problem for the propagation of the "start-down" front arises: its contact line is the place where the height is going to zero, so that the velocity there is null. In other words, such fronts cannot propagate at all. A first solution is to say that by breaking down it will create a shock, and then the velocity of this shock is given by conservation equations, without looking at any further detail. Another possibility is to say that the front is periodically breaking down and spreading, with a different law of motion when spreading, so that we have some kind of stick/slip motion. Yet another possibility is to set a slip velocity: a non-zero velocity limit for null height. This is what is usually done for liquids, but also in Ref. 3.

Experimentally we do not strictly speaking observe a shock at the "start-down" front, but a well-defined shape with a well-defined front angle, similar to wetting liquid fronts with a wetting angle. We also do not observe a visible stick/slip motion, but rather a continuous motion, with various velocities depending on the front height.

The case of the "start-up" fronts is different. The advective term may effectively create a shock. However, the grains spontaneously start to roll down if the angle becomes larger than ϕ_s. Thus, its slope should saturate and simply be this starting angle ϕ_s.

5.3. *"Stop-down" front propagation*

With a increasing velocity profile the "stop-down" front clearly flattens with time. But the fact that it propagates down implies a further condition: that for a small enough height (or velocity), the moving layer simply freezes. Otherwise, the front would just flatten out, but its foot should remain always at the same place.

5.4. *Simulation*

The consequence of the first observation of these four fronts is first that the mean velocity should be increasing with flow depth. The "stop-down" front also indicates that there must be a typical height or velocity under which the friction force becomes the static one. These ingredients are present in our model. Its numerical

[d]At this stage, more precise investigation is required to separate a linear velocity profile from a Bagnold one, but the way the "stop-down" front flattens (as $1/t$) is, for the moment, in favor of a linear velocity profile.

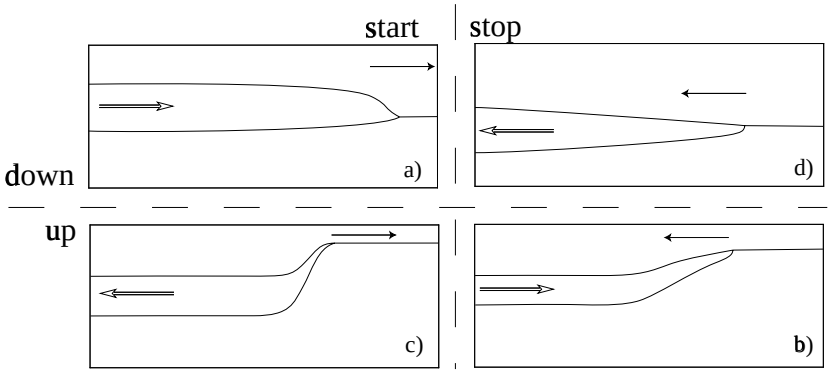

Fig. 9. The four types of fronts as obtained with numerical integration of our model. (a–d) as in Fig. 7.

integration indeed presents the four types of fronts with the expected characteristics, as shown in Fig. 9. In particular, we observe a "start-down" front propagating with a constant shape and velocity.

In our model, this result derives from the divergence of the grain velocity at ϕ_∞. We see that the slope of the free surface is continuously increasing when going to the front foot. Using, in our model, a local velocity gradient corresponding to the velocity of one bead, when the front foot reaches the angle ϕ_∞, then locally the velocity gradient becomes infinite. Physically, it just means that the grains start locally to jump and accelerate. Such gaseous grain, ahead of the front are indeed observed. Mathematically, we then have H going to zero, while Γ goes to infinity. The mean velocity $U = 1/2\Gamma H$ can thus tend, at the front foot, toward a constant value. Thus, the front can propagate with an arbitrary velocity. A consequence of this interpretation is that the front angle should always be precisely ϕ_∞.

6. Conclusion

We have seen that looking at the motion of a single bead and layer of beads gives much information on granular surface flows. The first point is the presence of the trapping of grains in the dip between the ones underneath. The second is that the complex grain motion results on average to the hysteretic friction laws. The third is the non-locality of the shocks in dense slow flows, as all the grains are in permanent contact. The fact that for a larger angle, a more rapid flow, or a different bottom, the contact line may become finite and small, could explain the difference between the velocity profiles observed for surface flows and chute flows. These points deserve further exploration.

The St-Venant approach seems to be satisfactory in the case of stationary granular surface flows if the hypothesis of a linear velocity profile with a velocity gradient given by the velocity of one grain is used. Its results are also compatible, at least qualitatively, with more demanding cases such as the four avalanche fronts. The

next work is to make a quantitative comparison. In particular, this model depends only on five parameters with well-defined physical meanings (see Fig. 2): the starting angle ϕ_s, the stopping angle ϕ_d, the jumping angle ϕ_∞, the freezing height H_{trap}, and a normalization constant γ (in front of the velocity). As these parameters can be obtained from several independent experiments, numerous cross checks are possible. Finally, a more distant goal would be to see how far these types of models can be extended, in particular in the case of geological flows. Is the inertial effect already present with the advective term derived from a linear velocity profile enough to describe these huge flows, or are further modifications needed?

References

[1] Ancey, C., Evesque, P. and Coussot, P., *J. Phys.* (*France*) **I6**, 725 (1996).

[2] Andreotti, B. and Douady, S., Selection of velocity profile and flowing depth in granular flows, *Phys. Rev.* **E63**, 031305 (2001).

[3] Aradian, A., Raphaël, E. and de Gennes, P.-G., Thick surface flow of granular materials: The effect of the velocity profile on the avalanches amplitude, *Phys. Rev.* **E60**, 2009 (1999).

[4] Azanza, E., Chevoir, F. and Moucheront, P., *J. Fluid Mech.* **400**, 199 (1999).

[5] Bagnolds, R. A., The shearing and dilatation of dry sand and the 'singing' mechanism, *Proc. R. Soc. London, Ser.* **A295**, 219–232 (1966).

[6] Bonamy, D., Faucherand, B., Planelles, M., Daviaud, F. and Laurent, L., Granular surface flows in a rotating drum: Experiments and continuous description, in *Powder & Grains 2001*, Kishino, Y. and Balkema, A. A., eds. (Amsterdam, 2001), p. 463; Bonamy, D., Daviaud. F. and Laurent, L., Experimental study of granular surface flows via a fast camera: A continuous description, to appear in *Phys. Fluids.*

[7] Bouchaud, J. P., Cates, M., Prakash, J. R. and Edwards, S. F., A model for the dynamics of sandpile surfaces, *J. Phys.* (*France*) **I4**, 1383 (1994).

[8] Boutreux, T., Raphael, E. and de Gennes, P. G., Surface flows of granular material: A modified picture for thick avalanches, *Phys. Rev.* **E58**, 4692 (1998).

[9] Daerr, A. and Douady, S., Two types of avalanche behaviour in granular media, *Nature* **399**, 6733 (1999).

[10] Daerr, A., Dynamical equilibrium of avalanches on a rough plane, *Phys. Fluids* **13**, 2115 (2001).

[11] De Barré Saint-Venant, A. J. C., Mémoire sur des formules nouvelles pour la solution des problèmes relatifs aux eaux courantes, *C. R. Acad. Sci.* (*Paris*) **31**, 283 (1850).

[12] Douady, S., Andreotti, B. and Daerr, A., On granular surface flow equations, *Eur. Phys. J.* **B11**, 131 (1999).

[13] Forterre, Y. and Pouliquen, O., Longitudinal vortices in granular flows, *Phys. Rev. Lett.* **86**, 5886 (2001).

[14] Jan, C. D., Shen, H. W., Ling, C. H. and Chen, C. L., *Proc. of the 9th Conf. On Eng. Mech. College Station* (Texas, 1992), p. 768.

[15] Jenkins, J. and Chevoir, F., Dense plane flow of frictional spheres down a bumpy, frictional incline, preprint (2001).

[16] Komatsu, T. S., Inagaki, S., Nakagawa, N. and Nasuno, N., Creep motion in a granular pile exhibiting steady surface flow, *Phys. Rev. Lett.* **86**, 1757 (2001).

[17] Metha, A., Luck, J. M. and Needs, R. J., Dynamics of sand piles: Physical mechanisms, coupled stochastic equations, and alternative universality classes, *Phys. Rev.* **E53**, 92 (1996).

[18] Mills, P., Loggia, D. and Tixier, M., Model for a dense stationary granular flow along an inclined wall, *Europhys. Lett.* **45**, 733 (1999).
[19] Pouliquen, O., On the shape of granular fronts down rough inclined planes, *Phys. Fluids* **11**, 1956 (1999).
[20] Pouliquen, O., Scaling laws in granular flows down rough inclined planes, *Phys. Fluids* **11**, 542 (1999).
[21] Prochnow, M., Chevoir, F. and Albertelli, M., in *13th International Conference on Rheology* (Cambridge, 2000).
[22] Quartier, L., Andreotti, B., Daerr, A. and Douady, S., On the dynamics of a grain on a model sandpile, *Phys. Rev.* **E62**, 8299 (2000).
[23] Rajchenbach, J., Continuous flows and avalanches of grains, in *Physics of Dry Granular Media*, Hermann, Hovi and Luding, eds. (Kluwer Academic, Nethterlands, 1998), p. 421.
[24] Ristow, G. H., Riguidel, F. X. and Bideau, D., *J. Phys.* (*France*) **I4**, 261 (1994).
[25] Savage, S. B. and Hutter, K., *J. Fluid Mech.* **199**, 177 (1989).
[26] Whitham, G. B., *Linear and Nonlinear Waves* (John Wiley & Sons, 1974).